Biexciton Dynamics in Alloy Quantum Dots

David Morgan, Ke Gong, Anne Myers Kelley and David F. Kelley*

Chemistry and Chemical Biology, University of California Merced,
5200 North Lake Road, Merced, CA 95343

Abstract

The biexciton Auger dynamics of alloyed $Zn_{1-X}Cd_XSe/ZnS$ and $Zn_{1-X}Cd_XSe/CdS$ core/shell nanoparticles are examined. A series of particles with increasing cadmium mole fractions are prepared by synthesizing ZnSe nanocrystals followed by cation exchange with cadmium oleate. This is followed by the low temperature deposition of a CdS or ZnS shell to passivate surface traps. The percent composition of cadmium in the core particles is determined from the absorption spectrum upon cation exchange, and the excited state dynamics are measured using power-dependent transient absorption spectroscopy. The biexciton lifetimes are controlled by Auger processes, and the results show that Auger recombination is faster for alloys than for either pure ZnSe or pure CdSe. The lifetimes go through a minimum at a composition that is approximately 10 – 40% cadmium. This behavior is assigned to partial hole localization at clusters of cadmium atoms in the alloy, which increases Auger rates through the same mechanism that is responsible for the strong size dependence of Auger processes in nanocrystals. The results can be semiquantitatively understood in terms of effective mass calculations of the hole wavefunctions on random (Cd,Zn)Se lattices of varying average compositions corresponding to alloyed nanocrystals of this size. We show that the hole wavefunction gradients (taken to be related to the Auger rates) also go through a maximum at approximately these alloy compositions.

Introduction

Biexciton dynamics are of great importance in any application of quantum dots (QDs) involving high rates of excitation, such as solar energy conversion and lighting in displays. Biexcitons are also formed as a result of multiple exciton generation, in which absorption of a high-energy photon results in the production of two electron-hole pairs. A biexciton Auger process is one in which an electron and a hole undergo a radiationless recombination, giving the energy to either the other electron or the hole. Due to the larger density of states in the valence band, the hole is typically the dominant receiving particle in the II-VI semiconductors. Auger recombination is typically fast compared to radiative relaxation and dominates the biexciton dynamics. Auger times are often found to scale approximately as the particle volume. This can be explained in terms of the momentum-forbidden nature of the Auger process for bulk semiconductors. The finite size of the QD results in the electron and hole wavefunction being composed of a superposition of different bulk wavefunctions having a range of momenta, which is simply an Uncertainty Principle consideration. This momentum distribution partially relaxes the momentum selection rule, making the Auger process partially allowed. The extent to which this happens depends on the spatial extent of the wavefunction and hence the particle size. Smaller particles have larger high-momentum components and hence faster Auger recombination rates. In addition, electron-hole Auger recombination occurs through a Coulombic interaction, the magnitude of which depends on the average electron-hole separation. Thus, there is a larger Coulomb matrix element associated with confining carriers to a smaller volume particle. The result of these factors is the approximate volume scaling of the biexciton lifetimes that is experimentally observed.[1]

The size of the electron or hole wavefunction can be affected by factors other than the particle size. We have recently shown that holes can trap at defects at the interface in core/shell QDs.[2] These trapped holes are far more spatially localized than band-edge holes and, as such, have much larger high momentum components. The result is that core/shell QDs having holes trapped at the core/shell interface exhibit Auger recombination rates that are several times faster than those lacking interfacial traps. In any ensemble of particles, some subset will have hole-trapping interfacial defects and show a fast component of the biexciton Auger decay. The remainder of the particles give the slow decay characteristic of band edge holes. Thus, ensemble transient absorption measurements typically yield biphasic Auger dynamics. We have shown that softening the core-shell interface reduces the density of these strain-induced defects and thereby greatly slows the Auger dynamics.

Another way to localize holes is through the introduction of impurities.[3, 4] This occurs at the first stages of alloying a semiconductor QD via cation exchange. We have very recently examined the extent of exciton-phonon coupling (EPC) in $Zn_{1-x}Cd_xSe$, x = 0 – 1.[4] The QDs exciton couples to the phonons through a Fröhlich mechanism. That is, if the nascent electron and hole have different spatial extents then there is an electric field associated with the electron-hole pair. The electric field displaces the atoms of the polar crystal along the optical phonon coordinates. Because of its smaller effective mass, the electron wavefunction typically has a slightly larger spatial extent than the hole. In pure, single material QDs this difference is minimal, and pure QDs exhibit relatively small Huang-Rhys parameters. Recent results indicate that QDs of both ZnSe and CdSe pure materials exhibit rather small electron-phonon couplings. The Huang-Rhys parameter is a quantitative measure of EPC, and ZnSe QDs give values on the order of 0.2 to 0.5, which is about a factor of 2 larger than what is obtained for CdSe QDs of similar size.[5] The $Zn_{1-x}Cd_xSe$ alloys show much stronger EPCs than either pure material. The key to this difference is that these are random, rather than uniform alloys. For small values of x, the Cd atoms can randomly cluster together, resulting in low energy valence band regions in the particle. Holes can localize at these regions,

resulting in large electric fields and hence large EPCs. We reported that the alloyed QDs exhibit much larger overtone to fundamental ratios in the Raman spectra than either of the pure materials, indicative of larger coupling of the exciton to the phonons.

These results suggest that other dynamics associated with more localized holes should also be observed in these alloyed QDs. The Auger rate depends on the extent to which the momentum selection rule is relaxed, i.e., the magnitude of the high momentum components comprising the hole wavefunction. These can be calculated by Fourier transforming the spatial wavefunction and evaluating the resulting wavefunction at the momentum corresponding to the exciton energy.[6-8] The qualitative conclusion is that the high momentum components are due to rapid spatial variation of the wavefunction and therefore increase with the spatial wavefunction gradients. Based on this simple consideration, we expect that the more localized hole of the alloys will result in faster biexciton Auger times. In this paper, we use transient absorption spectroscopy to measure the biexciton decay rates in a series of alloyed $Zn_{1-x}Cd_xSe$/CdS core/shell QDs. These experimental results are compared with calculated hole wavefunctions for random alloys with a specified average composition. We then evaluate the wavefunction gradients for comparison with the experimental results.

Experimental.

Chemicals.

Zinc stearate (Alfa Aesar, ZnO 12.5-14%), cadmium oxide (Aldrich, powder 99.5% trace metal basis), stearic acid (Sigma-Aldrich, analytic standard), oleylamine (Aldrich, technical grade), octylamine (Aldrich, 99%), 1-octadecene (ODE) (Aldrich, technical grade, 90%), Se powder (Alfa Aesar, 200 mesh, 99.999%), toluene (Alfa Aesar, ACS, 99.5%) and chloroform (Sigma-Aldrich, 99%) were used as received. Acetonitrile was purified by distillation over P_2O_5. Methanol (Acros Organics, 99+% extra pure) was distilled over iodine-activated magnesium before use.

Synthesis of ZnSe QDs and Cd cation exchange.

The alloyed core particles were synthesized by starting with pure ZnSe particles and performing a partial ion exchange with cadmium oleate. The ZnSe particles were synthesized as previously described.[5, 9] Reference 10 describes the particle synthesis and ion exchange procedures used to obtain the alloyed particles. Those authors use XRD, EELS, TEM and STEM-HAADF to characterize the alloyed particles and determine under what circumstances ion exchange results in complete alloying. The conditions that result in complete alloying have been used here and are the same as used in reference 4. Reference 4 also presents TEM images that confirm that the present synthesis accurately reproduces the results presented in reference 10.

ZnSe synthesis: 0.126 g (0.2 mmol) $Zn(stearate)_2$ and 5 mL ODE were loaded in a 25 mL 3-neck flask, evacuated for 10 minutes, then heated to 270 °C under N_2 flow. In a separate vial, 0.008 g (0.1 mmol) Se powder was dispersed in 1 mL ODE, evacuated for 2 minutes, sonicated for 5 minutes, then injected into the flask at 270 °C. After the initial injection, the reaction temperature was lowered to 240 °C for 10 minutes. The particles were grown using alternating injections of 0.1 mL of 0.1M Se and $Zn(acetate)_2$ at 240 °C until they reached 3.7 nm in diameter as determined by the absorbance spectra. An aliquot was taken, then the temperature was raised to 270 °C. Additional Se and $Zn(acetate)_2$ was injected every 15 minutes until the particles reached 4.5 nm in diameter.

Cation exchange: The ZnSe particles were purified as follows. 0.2 mL TBP, 0.2 mL octylamine, and 2 mL chroloform were added to 1 mL of the raw reaction mixture, and the resulting solution was heated to 50 °C. 2 mL of acetonitrile was then added to precipitate the particles, which were then centrifuged,

decanted, and resuspended in 1 mL of chloroform. This procedure was repeated three times, then the particles were resuspended in 3 mL ODE and 0.5 mL oleylamine and loaded in a 25 mL 3-neck flask. The temperature was then raised to 220 °C for the exchange reaction. A 0.1M solution of $Cd(oleate)_2$ was prepared by dissolving 0.026 g CdO in 0.7 mL ODE and 0.3 mL oleic acid at >200 °C under an N_2 atmosphere. After cooling, increments of 0.05 mL of the 0.1M $Cd(oleate)_2$ solution were added to the solution, reacting for 3 minutes between each addition until the desired alloy composition was reached.

Shell deposition: The core alloyed particles were purified by repeated precipitation as described above, then resuspended in 3 mL ODE and 0.5 mL oleylamine for either CdS or ZnS shell deposition. ZnS shells were deposited by SILAR[11] using an equimolar mixture of TOP:S and $Zn(acetate)_2$ and reacting at 235 C. CdS shells were deposited using a single source precursor cadmium diethyldithiocarbamate, $Cd(DDTC)_2$ at 140 C.[12] For both ZnS and CdS shells, the amounts of the precursors were calculated to give approximately one monolayer of the shell.

Optical Measurements.

Transient absorption measurements were obtained at several different excitation intensities using an apparatus described in reference 13. Samples were held in rapidly stirred 1 cm cuvettes and had an absorbance at the excitation wavelength of about 0.7−1.0. In a typical low power experiment, 0.3 μJ, 387 nm excitation pulses at a repetition rate of 1 kHz were focused to a spot size of 1.5 mm. Higher power experiments used excitation pulses having intensities between 1.0 and 1.5 μJ/pulse. The sample was probed with a white light continuum and the spectrum dispersed on a LN2 cooled CCD. Static luminescence spectra were measured on a Jobin-Yvon Fluorolog 3 using a CCD detector. Static absorption spectra were measured using a Cary 50 UV-vis spectrophotometer.

Results

Absorption spectra of 3.7 nm alloyed particles at various stages of ion exchange are shown in Figure 1A. The original ZnSe particles show a well defined absorption maximum at 402 nm. The exciton energy of ZnSe QDs varies with size in a known manner[14] and this establishes the ZnSe particle diameter as 3.7 nm. The absorption spectra shift to the red as zinc to cadmium ion exchange occurs and the extents of ion exchange are determined by the magnitudes of these shifts. We also note that due to the difference in lattice parameter (CdSe is 6.5% larger than ZnSe), the particles increase from 3.7 to 3.9 nm as ion exchange occurs. The exciton energy (in eV) varies with composition in a nonlinear fashion – there is a finite amount of "optical band-bowing" in these alloys. For the case of ZnSe and CdSe alloys, the band-bowing parameter is about 0.49 eV and the bandgap energy as function of composition is given by[15]

$$E_g(Zn_{1-x}Cd_xSe) = x\,E_g(CdSe) + (1-x)\,E_g(ZnSe) - 0.49\,x\,(1-x) \qquad \text{Eqn. 1}$$

where $E_g(ZnSe)$ and $E_g(CdSe)$ are the exciton energies in pure ZnSe and CdSe QDs. For 3.7 nm ZnSe particles, the exciton energy is obtained from the absorption spectrum and is taken to be $E_g(ZnSe) = 3.08$ eV. Sizing curves[16] give for 3.9 nm CdSe particles give $E_g(CdSe) = 2.14$ eV. These spectra are very similar to those in reference 4, indicating that the ion exchange process is quite reproducible.

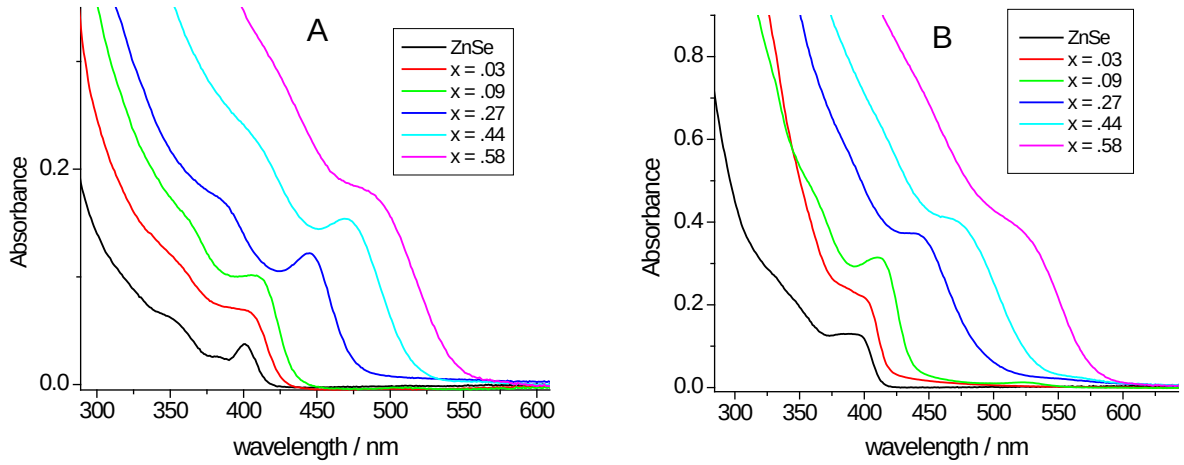

Figure 1. (A) Scaled absorption spectra of 3.7 nm $Zn_{1-x}Cd_xSe$ particles. (B) Scaled absorption spectra of 3.7 nm $Zn_{1-x}Cd_xSe$/ZnS core/shell particles. The cadmium mole fractions, x, corresponding to the different spectra are also indicated.

Following alloying by ion exchange, a thin ZnS or CdS shell is deposited onto the alloyed core particles. The CdS shells are deposited at a very low temperature (140 °C) to avoid having further ion exchange or diffusion change the composition or radial composition profile. This is not a problem for the deposition of a ZnS shell, and in this case the shells were deposited at higher temperature. Deposition of a thin ZnS shell shifts the spectra slightly to the red as shown in figure 1B. This is particularly true for spectra of the particles having greater concentrations of cadmium. The spectral shift occurs for a combination of two reasons. Some of the shift is due to penetration of the (primarily electron) wavefunction into the ZnS shell, reducing the amount of quantum confinement. However, for the most exchanged particles (x = 0.58) this shift is close to 30 nm, which is too large to be explained by wavefunction delocalization into the ZnS. We conclude that some of the red shift comes from the reaction of residual cadmium adsorbed on the particles that comes through the purification process. This cadmium reacts with the TOP:S, forming a sub-monolayer shell of CdS between the CdSe core and the ZnS shell.

The composition of an alloy QD can be determined from the wavelength of the exciton maximum in the absorption spectrum, using equation 1. Figure 1 shows that some of the spectra are sufficiently broadened that the exciton maxima are not well defined, which makes the determination of the average extent of exchange somewhat uncertain. This broadening occurs from exchange inhomogeneity (different particles have different zinc versus cadmium compositions) and is exacerbated by spectral congestion caused by the higher energy transitions. In the crude approximation that the probability of a zinc to cadmium exchange is independent of the extent of alloying, the number of cadmiums in each particle at any average extent of alloying follows a binomial distribution, and it is the width of this distribution that is the largest source of absorption spectrum broadening. However, all of the transient absorption spectra have a bleach feature which corresponds only to the lowest energy transition – spectral congestion from higher energy transitions does not contribute to the bleach. As a result, these spectra have very well defined bleach maxima corresponding to the lowest energy excitons. We find that in cases where the static absorption spectra have well defined maxima, the bleach maxima closely correspond to the same

wavelength. To avoid ambiguity resulting from broad static absorption spectra, the spectral positions of the bleach features in the transient absorption spectra are used to determine the particle compositions. The values of x shown in figure 1 were determined in this way.

Throughout the present studies, all transient absorption (TA) kinetics were obtained on particles having a thin shell of either ZnS or CdS. Examples of the power dependent TA results on 3.7 nm ZnSe particles having a 1 monolayer CdS shell are shown in figure 2.

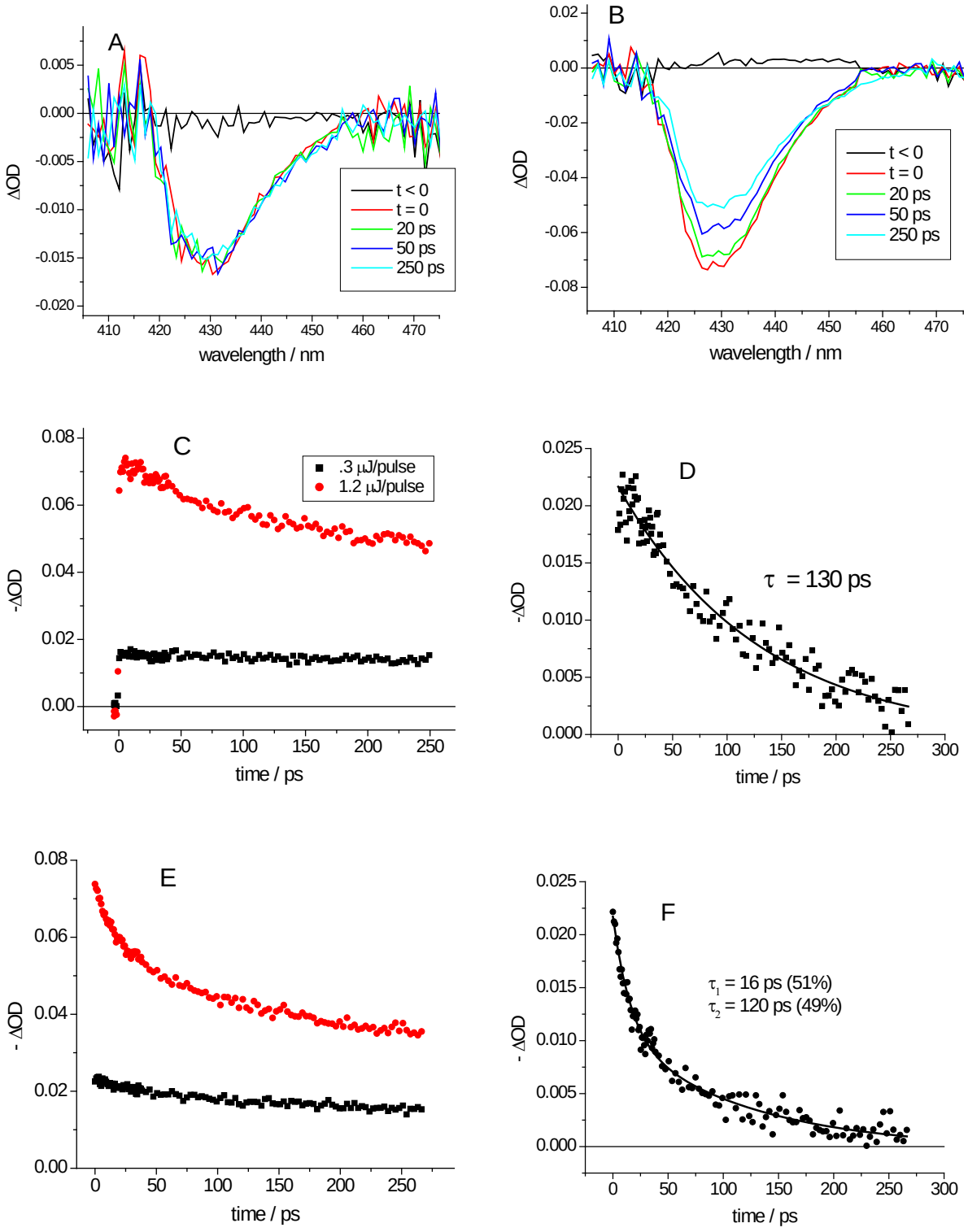

Figure 2. Representative TA results for pure 3.7 nm ZnSe/CdS measured at excitation fluences of (A) 0.3 μJ/pulse and (B) 1.2 μJ/pulse. (C) The power dependent 1S-1S exciton bleach kinetics, and (D) the biexciton decay. Panels E and F are the same as C and D, except corresponding to alloyed particles

having a composition of $Zn_{0.82}Cd_{0.18}Se/CdS$. Panels D and F also show fitted decay curves having the indicated time constants. Pure CdSe/CdS of this size gives a biexciton decay of about 120 ps.

Figure 2A shows that the low power TA bleach exhibits a well defined maximum at about 430 nm. Figure 2B shows very similar higher power TA spectra, having a larger magnitude bleach and a maximum observed at a similar wavelength. The presence of the CdS shell delocalizes the conduction band electron, reducing the extent of quantum confinement. The shell is quite thin (about 1 monolayer) so this shifts the ZnSe absorption maximum about 30 nm (0.20 eV) to the red. The low and high power kinetics at the bleach maximum are shown in figure 2C, and these plots make clear the reason for depositing a thin passivating shell. The CdS (or ZnS) shell passivates surface states involved in carrier trapping. Thus, unpassivated particles exhibit fast components in the low power decay kinetics. This is particularly true for the pure ZnSe particles and alloyed particles having small cadmium mole fractions. Such carrier trapping processes can also occur with biexcitons and therefore have the potential to confuse the measurements of the biexciton Auger rates. Figure 2C shows that the low power TA kinetics are very close to flat on this timescale, having no discernible fast decay components. Biexciton kinetics are obtained from a comparison of the low and high power bleach recovery kinetics. Specifically, the kinetics associated with absorption of two photons can be obtained from the difference between the high and low power results, where the low power results are scaled to match the high power results at times longer than the biexciton decay, greater than about 200 ps. Taking the difference between the high and scaled low power decays assumes that two photon excitation relaxes to the same states as are produced by one photon absorption. This is the usual approach and there is no reason to believe it is not completely valid here.[17] The difference kinetics correspond to the biexciton decay and are shown in figure 2D. Fitting this curve shows that within the signal to noise ratio, the biexciton decays with a single exponential having a time constant of 130 ps. This decay time is similar to what is expected for biexciton decays in comparably sized CdSe QDs.

Analogous TA results have been obtained for the alloyed QDs, as shown in figure 2E and 2F. In this case, the particle core composition corresponds to $x = 0.18$ and the particles have a comparable, one monolayer CdS shell. The low power bleach decay kinetics (figure 2E, black dots) are relatively flat on this time scale, having only a small amplitude decay component of approximately 100 ps. The biexciton kinetics (figure 2F) show a strongly nonexponential decay. These kinetics can be fit to a biexponential having 16 ps and 120 ps decay components with approximately equal amplitudes. Due to the limited range of the kinetic scans, there is considerable uncertainty in time constant of the slow component and the slow component could be equally well fit with a somewhat faster decay time. Comparable results are obtained with particles having a larger (4.5 nm diameter) core and a comparable one monolayer CdS shell. In this case the biexciton Auger times are all approximately a factor of two larger than obtained from the 3.7 nm particles as would be expected for volume scaling. A comparison of the biexciton Auger kinetics as a function of composition for the 3.7 and 4.5 nm particles is shown in figure 3. The most remarkable aspect of these results is that the alloyed particles show a fast component of the biexciton decay that is absent in either pure ZnSe or pure CdSe. This component is almost an order of magnitude faster than the pure ZnSe decay and constitutes about 50% of the biexciton decay.

Somewhat more complicated results are obtained for ZnSe and alloyed QDs having a ZnS shell. The ZnS shell does not completely passivate the surface carrier traps and the low power TA results show a significant decay component (about 30% of the total) having a time constant of 10 – 20 ps. Despite this complication, biexciton decays can be obtained from the power dependent TA kinetics using the same

procedure as outlined above. The pure materials and alloy results are also shown in figure 3. In the case of these 3.7 nm diameter ZnSe/ZnS (the x = 0 case) particles having the ZnS shell, the absorption bleach is quite far to the blue (about 405 nm) which is close to the blue spectral limit of the TA apparatus, limiting the signal to noise ratio of these kinetics. Despite this difficulty, figure 3C shows that close to a single exponential decay is obtained for pure ZnSe/ZnS. The important result from the TA results on the ZnS coated particles is that the 10 – 40% cadmium alloy particles exhibit a biphasic decay with the short component being much shorter than either of the pure materials.

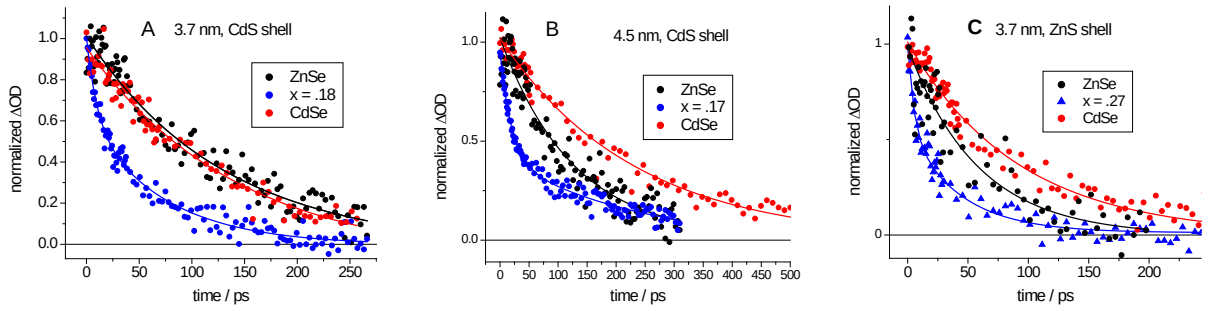

Figure 3. Normalized biexciton decays for (A) 3.7 nm and (B) 4.5 nm diameter alloyed particles passivated with a CdS shell, and (C) 3.7 nm particles passivated with ZnS. The pure ZnSe and CdSe decays are fit to single exponentials and the alloyed particles are fit to biexponentials. The pure ZnSe and CdSe decay times and alloy fast components given in figure 4. The alloy slow components correspond to the pure ZnSe decay time.

The results in figure 3 show that in all cases the biexciton decays of the pure ZnSe and pure CdSe give close to single exponential decays, with a time constant on the order of 100 ps. The biexciton kinetics of the alloys are more complicated, showing strongly nonexponential decays when the cadmium fraction is about 10 – 40%. This is independent of particle size or whether the particle has a CdS or ZnS shell. At larger cadmium fractions (x > 0.40), single exponential decays are obtained, but when the alloy is close to equal amounts of zinc and cadmium, the time constants are significantly less than what is obtained for pure CdSe. The single exponential times constants obtained for the pure ZnSe and CdSe and the x > 0.4 alloyed particles are summarized in Figure 4. Also shown in figure 4 are the fast component decay times in the cases where the alloyed particles give a biexponential decay. Thus, figure 4 shows the fastest biexciton decay component for all the particle compositions. In all cases the fast component decay time goes through a minimum at a composition of about 10% to 40% cadmium. At this minimum, the amplitudes of the fast and slow components are roughly equal.

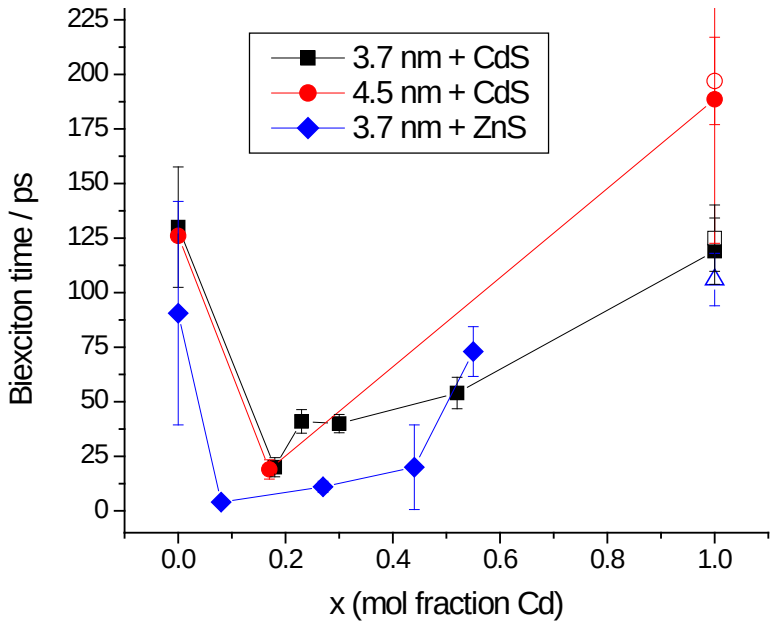

Figure 4. Fast decay component times for three different types of alloy QDs as a function of composition. Closed symbols: ZnSe and cation exchanged particles. Open symbols: pure CdSe with a CdS or ZnS shell. Error bars correspond to 2σ uncertainties obtained from the least-squared fitting of the decays.

Discussion

Qualitative considerations.

The results presented above may be summarized as a few simple observations.

1. The biexciton kinetics of pure ZnSe or CdSe follow single exponential decays with time constants on the order of 100 ps.

2. Biexciton Auger times of the alloyed particles do not change smoothly with composition. Alloyed particles having compositions in the range of 10 – 40% cadmium show biphasic decays. The fast component decay times show a distinct minimum in the range of 10 – 40 % cadmium and these components are about an order of magnitude faster than pure ZnSe or CdSe. This observation is independent of particle size. For these particles, the biphasic decays have slow components that are comparable to, or slightly faster than the pure materials. The fast and slow components have approximately equal amplitudes.

3. The biexciton kinetics of alloyed particles having compositions greater than 40% cadmium exhibit decays that can be fit to single exponentials having time constants that are longer than the fast components at x = 1.0 – 0.4, but significantly shorter than the decay times of pure ZnSe or CdSe.

The biexciton decay kinetics of pure ZnSe and CdSe QDs are straightforward. To the best of our knowledge, biexciton Auger times in ZnSe QDs have not previously been reported. However, based on the similarity with CdSe (similar effective masses, dielectric constants, etc.), one would not expect that Auger recombination times would be vastly different, and indeed, we see ZnSe Auger decay times that are comparable, or at most a factor of two faster. The Auger times obtained following complete ion exchange (nominally pure CdSe) are consistent with core/shell QDs, obtained from comparably sized

pure zincblende CdSe cores. The biexciton decay times in these QDs approximately follow volume scaling and previously reported size dependent CdSe Auger times.[13, 18]

We suggest that the faster and nonexponential decays observed for the alloyed QDs can be understood in terms of a few simple considerations. The key idea is that these are random, rather than uniform alloys. If a small fraction, say 20%, of the zinc atoms are randomly replaced with cadmiums, then there will be regions in each of the particles where the cadmium concentrations are locally higher or lower than the average. Due to the valence band offset and band-bowing effects, the regions of higher cadmium concentrations will have a lower energy valence band. These spatial variations of the valence band energy result in partial localization of the holes, and the extent of hole localization is crucial in determining the biexciton Auger rate. This is because Auger recombination is a nominally momentum forbidden process, and it is the high momentum components that relax this selection rule and thereby increase the biexciton Auger rate.[6-8] The momentum components of a wavefunction are given by the Fourier transform and high frequency Fourier components (i.e., high momentum components) result from regions of the wavefunction having large gradients. As a result, spatial localization of the wavefunctions increases the maximum gradient of the wavefunction and results in high momentum components and faster biexciton Auger recombination.

The observed trend in Auger times is similar to what is observed for the electron-phonon couplings in alloyed particles, and we suggest this occurs for what is essentially the same reason. In a previous paper, we found that $Zn_{1-x}Cd_xSe$ alloys[4] gave much larger electron phonon couplings (EPCs) than either pure ZnSe[5] or pure CdSe.[19-21] EPC occurs through a Fröhlich mechanism, whereby the optical phonons of a polar crystal are excited by the electric field produced by differential overlap of the electron and hole wavefunctions.[22] Random concentration variations cause spatial variations in both the valence and conduction band potentials. However, due to the much smaller effective mass of the electron,[23] much less electron localization occurs. The overall result is that the internal electric field is dominated by spatial variations in the valence band potential causing partial hole localization. This greatly increases the spatial differences between the electron and hole wavefunctions and therefore increases the magnitude of the electric field of the exciton, increasing the EPC. The same spatial variations and partial hole localization produce high momentum components of the hole wavefunction, increasing the biexciton Auger rate.

Calculations of hole density gradients as a function of composition.

The above qualitative statements can be made more quantitative through hole wavefunction calculations that consider the alloy energetics. The potential used in solving the Schrödinger equation is the (linear) average of the valence bands associated with the zinc and cadmium atoms in the nanocrystal. The local concentration of each type of atom varies spatially, giving rise to the spatially dependent valence band potential. The ZnSe and CdSe valence bands are not much different in energy, 6.22 and 6.0 eV below the vacuum level, respectively.[15] However, neither the band gap nor the valence band energy varies linearly with composition, i.e., $Zn_{1-x}Cd_xSe$ alloys exhibit optical band bowing.[15, 24-26] Optical band bowing is typically characterized by a single parameter (as in equation 1) that gives the band gap as a function of composition. Some of this composition dependence is in the conduction band and some is in the valence band. Calculations indicate that in the case of $Zn_{1-x}Cd_xSe$ alloys most of the variation is in the conduction band, but a significant amount is also in the valence band.[15] These calculations indicate that the valence band energy can be characterized by a band-bowing parameter of about 0.14 eV, as depicted in figure 5.

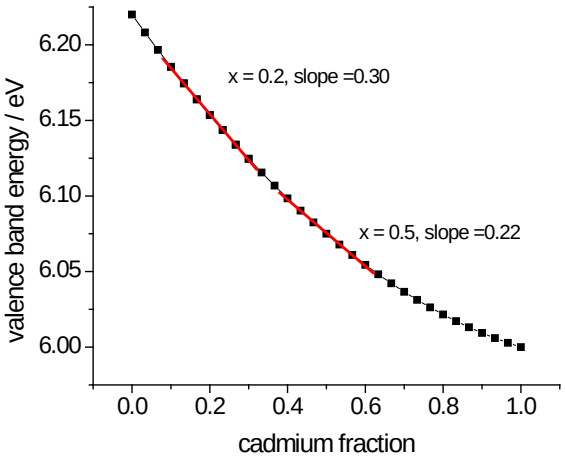

Figure 5. Valence band energy as a function of composition for bulk $Zn_{1-x}Cd_xSe$. The CdSe and ZnSe valence band energies are taken to be 6.0 and 6.22 eV, respectively, and the value of the valence band bowing parameter is taken to be 0.14, following reference 15. The slopes of the curve at x = 0.20 and x = 0.50 are also indicated as red lines.

The curve in figure 5 ignores quantum confinement, but because the quantum confinement energy for holes in QDs is rather small, we assume that the same curve can be applied to QDs with an overall shift of the energy axis. We conclude that if the difference in valence band potential energy between cadmium and zinc atoms is taken to be the derivative of the valence band energy versus composition curve, then this gives the correct spatially dependent potentials in the Schrödinger equation. In the present case, the potential differences are 0.30 eV at 20% Cd and 0.22 eV at 50% Cd, see figure 5. These were the values employed in our calculations of the excitonic hole densities in QDs. We note that these values do not give the correct absolute values of the valence band energies, but they properly capture the change in valence band energy with composition at a particular composition, and that is what matters for determining the spatial extent of the hole wavefunction.

Using these energetics, the hole wavefunctions can be calculated by either of two approaches. The simplest approach uses a random number generator to assign the positions of the cadmium and zinc atoms and first order perturbation theory to calculate the wavefunction. This calculation is done as follows. We start by constructing a 3.3 nm diameter sphere (r_0 = 1.65 nm) containing about 400 atoms by cutting this out from a face-centered-cubic lattice having the ZnSe lattice parameter. This corresponds to the metal atom positions in the QD. CdSe has a somewhat larger (about 6.5%) lattice parameter than ZnSe, and the alloy lattice parameter is taken to vary linearly with composition. In the absence of cadmium atoms, the hole wavefunctions are simply given by the particle-in-a-sphere wavefunctions, $\Psi_{nlm} = j_l(\alpha_{l,n} r / r_0) Y_l^m(\theta,\varphi)$, where j_l is the *l'th* spherical Bessel function having its *n'th* root at $\alpha_{l,n}$, $Y_l^m(\theta,\varphi)$ is a spherical harmonic and r_0 is the particle radius. The ground wavefunction is the 1S function, $\Psi_{100} = j_0(\alpha_{0,1} r / r_0) Y_0^0(\theta,\varphi)$. The energies of these states are given by $E_{n,l} = \frac{\hbar^2 \alpha_{l,n}^2}{2 m_{eff} r_0^2}$ where the hole effective mass is taken to be $m_{eff} = 2.9 m_e$, the value found to best reproduce the optical spectra of CdSe in a two-band model.[27]

Calculations are performed for approximately 20% and 50% cadmium. For a 20% cadmium alloy, 20% of the lattice points are chosen at random and assigned an energy of 0.30 eV and the remaining points are assigned an energy of zero. This gives the alloy potential, *V(x,y,z)*, which is defined at the lattice points. The above spatially-dependent potential is taken to be a perturbation that mixes the 1S hole state with the 2S and 1P states. The final state is given by the first order perturbation expression, where the coupling is calculated numerically over the grid of the 400 lattice points. The calculated hole wavefunctions are then written as the initial 1S wavefunction plus the sum of four additional terms:

$$\Psi = \Psi_{1S} + \frac{\langle \Psi_{1S} | V | \Psi_{1Px} \rangle}{E_{1P} - E_{1S}} \Psi_{1Px} + \frac{\langle \Psi_{1S} | V | \Psi_{1Py} \rangle}{E_{1P} - E_{1S}} \Psi_{1Py} + \frac{\langle \Psi_{1S} | V | \Psi_{1Pz} \rangle}{E_{1P} - E_{1S}} \Psi_{1Pz} + \frac{\langle \Psi_{1S} | V | \Psi_{2S} \rangle}{E_{2S} - E_{1S}} \Psi_{2S}$$

This final function can be differentiated to give the spatially dependent gradient. Maximum gradients obtained in this way for several 20% and 50% alloys are shown in figure 6, plotted as a function of composition.

An alternative and somewhat more realistic approach to this problem is as follows. We begin by constructing a ZnSe zincblende crystal and cutting out a 3.3 nm diameter QD containing 798 atoms ($Zn_{399}Se_{399}$). Approximately 20% or 50% of the zinc atoms are randomly replaced by cadmium using a random number generator. We have calculated twelve different structures with 17-23% Cd and twelve structures with 46-54% Cd. The geometry of each structure is then energetically minimized using the GULP program and the force field described in reference 4. The valence band potential energy is assumed to vary with position as the weighted average of the four nearest cations, thus making the potential energy lower in Cd-rich regions of the structure than in Zn-rich regions. As before, the kinetic energy is taken as that of a hard-walled particle in a sphere with radius equal to the radius of the QD and the hole effective mass is taken to be $m_h = 2.9m_e$. The hole wavefunctions are calculated by diagonalizing the Hamiltonian in a basis of the particle in a sphere wavefunctions (spherical harmonics up to $l = 4$ multiplied by the spherical Bessel functions for $n = 0$ to 2, a total of 75 basis functions). The gradients are then calculated numerically on a sufficiently small grid such that reduction of the grid volume elements does not change the calculated results. The calculated maximum spatial gradient of the hole wavefunction for ~3.3 nm diameter QDs that are approximately 20% Cd, 50% Cd, and pure ZnSe are shown in figure 6 and the corresponding hole densities for a pure ZnSe QD and for several representative ~20% Cd QDs are shown in Figures 7 and 8.

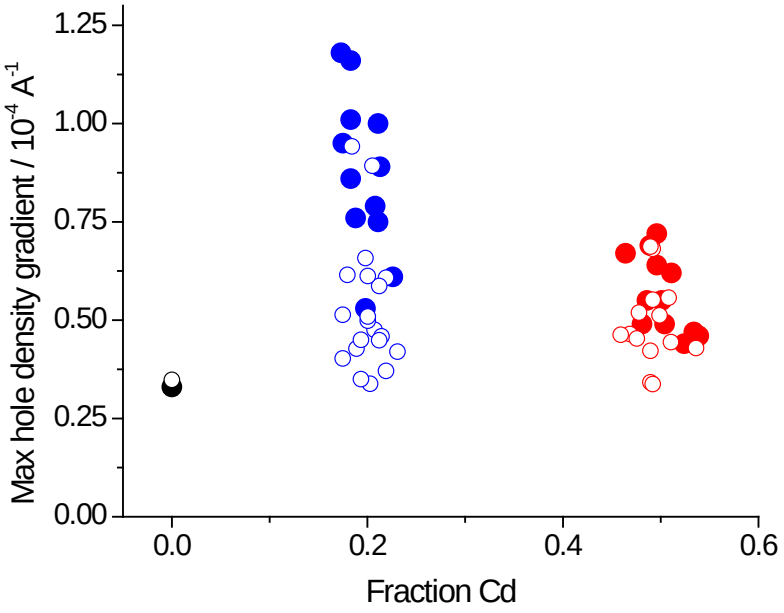

Figure 6. Calculated maximum hole density gradient as a function of fraction of cadmium in 3.3 nm QD random alloys. Points calculated from the perturbation and variational methods are shown as open and solid dots, respectively.

The two calculational approaches, compared in Figure 6, show very similar results. A larger gradient indicates more rapidly varying components of the hole wavefunction, which we associate with higher momentum components and a faster Auger recombination rate. Both 20% and 50% alloyed QDs show generally larger maximum gradients than the single-component QDs, and the gradients are generally larger for the 20% Cd structures than for the 50% ones. It is important to note that there is also a rather large spread in maximum gradient among structures having roughly the same composition. This is due to the random (rather than uniform) nature of the alloy. We note that the variational calculation shows somewhat larger gradients than the perturbation calculation. There are two principal differences between the two calculational approaches. First, the variational approach optimizes the local geometry, rather than taking the entire lattice to vary uniformly with composition. In terms of calculating a wavefunction gradient, this is expected to be a small effect. Second, the variational approach uses a larger basis set for expansion of the final wavefunction. The terms having larger values of n and l contribute functions having more rapid spatial variations, thus giving somewhat larger gradients.

The results in figure 6 are consistent with the experimental observation of the alloys having a range of Auger recombination times, with the fastest times in the alloys being much faster than in either pure CdSe or pure ZnSe. These calculations are also consistent with somewhat faster recombination in 20% compared to 50% alloys. In addition, we note that the dispersion of gradients for x = 0.2 is considerably larger than with x = 0.5. This is also consistent with our experimental results in which the x = 0.5 – 0.6 decays are fit with a single exponential, whereas the x = 0.10 – 0.40 results in all cases must be fit to a biexponential.

The plots in Figures 7 and 8 show color-coded representations of the hole density in each atom for a pure QD and for six of the structures with approximately 20% Cd, as calculated by the variational method described above. The hole density plotted in figure 7 is very close to spherically symmetric. In contrast, the plots in figure 8 clearly show the loss of spherical symmetry of the hole function of the alloyed particles. This is because the alloyed QD valence band potential varies with position in a manner that is not, in general, spherically symmetric, so the hole densities are also distorted from spherical symmetry. Similar distortions occur for the electron densities (not shown), but these are smaller because the much smaller effective mass of the electron makes it more difficult to localize. Thus, relatively small potential variations introduced by compositional variations of alloys can introduce sufficient valence band potential gradients to dramatically affect the QD photophysics.

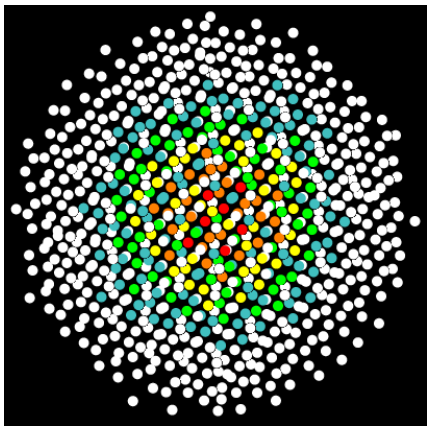

Figure 7. Color-coded hole densities on each of the atoms (white, cyan, green, yellow, orange, red representing increasingly high hole density) for a pure CdSe QDs.

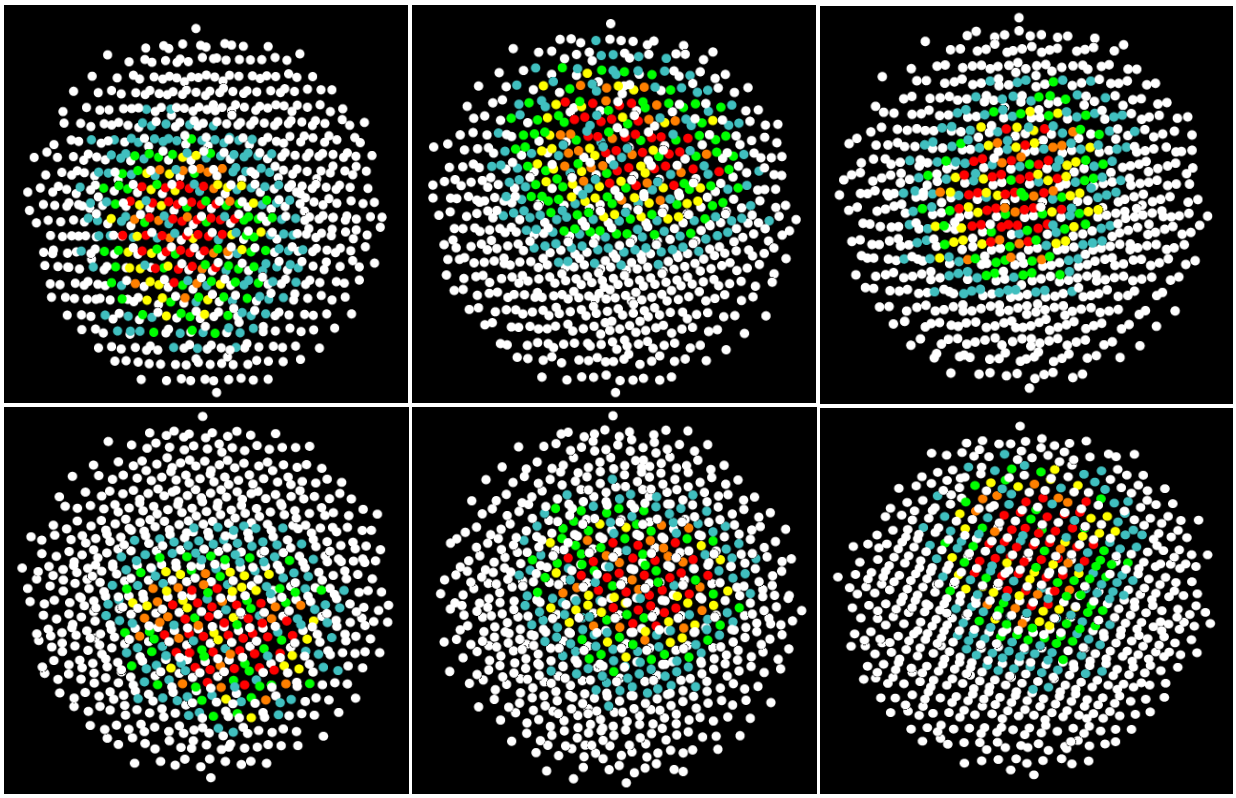

Figure 8. Same as figure 7 for six QDs of approximate composition $Cd_{0.2}Zn_{0.8}Se$.

Comparison of figure 7 with figure 8 shows the random alloying results in distortions of the hole wavefunction that are fairly small – the functions plotted in figure 8 are not very far from being spherically symmetric. This is consistent with simple calculations of the spatial variations of the valence band potential. For the case of x = 0.20, the variation of the valence band potential from one part of the particle to another is on the order of 20 meV, which seems like a very small energy. However, an interesting perspective results from the comparison of this energy difference and these wavefunctions with energy differences and wavefunctions calculated for the particle in a dipolar electric field. The wavefunction distortions created from valence band inhomogenieties are comparable to those that would be caused by putting the particle in a rather large external electric field, on the order of 10^7 V/m.

The calculation of the electric field that is equivalent to the valence band potential gradient allows us to comment on the magnitude of electric fields associated with charged ligands adsorbed on the particle surface. An equal dipolar component of the internal electric field would be created by adsorbing an uncompensated charge of 0.1 of an electron charge on the surface of the particle.[28] This result suggests that if the charge were uncompensated, adsorption of charged surface ligands (such as an alkylcarboxylate) would dramatically change much of the particle photophysics, especially dynamic quantities such as EPCs and Auger rates. However, this is not observed – Auger rates and measured EPCs are essentially independent of the nature of the surface ligands.[29] The conclusion is that QDs do not have uncompensated charged ligands on the surfaces. When charged ligands are attached to the particles in nonpolar solution, they are almost completely charge compensated by adsorption of counter ions.

Conclusions

Several conclusions follow from the results presented here.

- The biexciton Auger recombination kinetics of pure ZnSe and CdSe QDs follow single exponential decays. The decay times of both are on the order of 100 ps, with the CdSe giving somewhat slower decays.
- $Zn_{1-x}Cd_xSe$ alloyed QDs show more complicated decay kinetics, having slow and fast components of approximately equal amplitudes. The slow components have about the same decay times as the pure materials and the fast components are about an order of magnitude faster.
- The experimental results can be understood in terms of random, rather than uniform alloys, in which there are regions of locally higher and lower cadmium concentration. Because of the valence band offset and band-bowing effects, the holes are partially localized in the regions of higher cadmium concentration. This partial hole localization facilitates faster Auger recombination kinetics.
- These results are consistent with recently-reported resonance Raman results that also indicate partial hole localization.
- Partial hole localization can be semi-quantitatively understood through wavefunction calculations on random alloy structures.

These studies indicate that localized charges in general will have profound effects on QD exciton dynamics. Several studies to examine these effects are underway and will be reported in later papers.

Corresponding Author

*E-mail: dfkelley@ucmerced.edu

ORCID

David F. Kelley: 0000-0002-4076-7965

Anne Myers Kelley: 0000-0002-4073-109X

Notes

The authors declare no competing financial interest.

Acknowledgement

This material is based upon work supported by the U.S. Department of Energy, Office of Science, Office of Basic Energy Sciences, under award number DE-FG02-13ER16371 and by NSF grant CHE-1506803.

References

1. Klimov, V. I.; McGuire, J. A.; Schaller, R. D.; Rupasov, V. I., Scaling of Multiexciton Lifetimes in Semiconductor Nanocrystals. *Phys. Rev. B* **2008,** *77*, 195324 - 195324.
2. Beane, G. A.; Gong, K.; Kelley, D. F., Auger and Carrier Trapping Dynamics in Core/Shell Quantum Dots Having Sharp and Alloyed Interfaces. *ACS Nano* **2016,** *10*, 3755-3765.
3. Avidan, A.; Oron, D., Large Blue Shift of the Biexciton State in Tellurium Doped CdSe Colloidal Quantum Dots. *Nano Lett.* **2008,** *8*, 2384-2387.
4. Gong, K.; Kelley, D. F.; Kelley, A. M., Nonuniform Excitonic Charge Distribution Enhances Exciton–Phonon Coupling in ZnSe/CdSe Alloyed Quantum Dots. *J. Phys. Chem. Lett.* **2017,** *8*, 626-630.

5. Gong, K.; Kelley, D. F.; Kelley, A. M., Resonance Raman Spectroscopy and Electron–Phonon Coupling in Zinc Selenide Quantum Dots. *J. Phys. Chem. C* **2016,** *120*, 29533-29539.
6. Cragg, G. E.; Efros, A. L., Suppression of Auger Processes in Confined Structures. *Nano Lett.* **2010,** *10*, 313.
7. Climente, J. I.; Movilla, J. L.; Planelles, J., Auger Recombination Suppression in Nanocrystals with Asymmetric Electron-Hole Confinement. *Small* **2012,** *8*, 754-759.
8. Vaxenburg, R.; Rodina, A.; Shabaev, A.; Lifshitz, E.; Efros, A. L., Nonradiative Auger Recombination in Semiconductor Nanocrystals. *Nano Letters* **2015,** *15*, 2092-2098.
9. Pu, C.; Zhou, J.; Lai, R.; Niu, Y.; Nan, W.; Peng, X., Highly Reactive, Flexible Yet Green Se Precursor for Metal Selenide Nanocrystals: Se-Octadecene Suspension (Se-SUS). *Nano Research* **2013,** *6*, 652-670.
10. Groeneveld, E.; Witteman, L.; Lefferts, M.; Ke, X.; Bals, S.; Tendeloo, G. V.; de Mello Donega, C., Tailoring ZnSe-CdSe Colloidal Quantum Dots via Cation Exchange: From Core/Shell to Alloy Nanocrystals. *ACS Nano* **2013,** *7*, 7913.
11. Li, J. J.; Wang, Y. A.; Guo, W.; Keay, J. C.; Mishima, T. D.; Johnson, M. B.; Peng, X., Large-Scale Synthesis of Nearly Monodisperse CdSe/CdS Core/Shell Nanocrystals Using Air-Stable Reagents via Successive Ion Layer Adsorption and Reaction. *J. Am. Chem. Soc.* **2003,** *125*, 12567 - 12575.
12. Nan, W.; Niu, Y.; Qin, H.; Cui, F.; Yang, Y.; Lai, R.; Lin, W.; Peng, X., Crystal Structure Control of Zinc-Blende CdSe/CdS Core/Shell Nanocrystals: Synthesis and Structure-Dependent Optical Properties. *J. Am. Chem. Soc.* **2012,** *134*, 19685−19693.
13. Gong, K.; Kelley, D. F., Surface Charging and Trion Dynamics in CdSe-Based Core/Shell Quantum Dots. *J. Phys. Chem. C* **2015,** *119*, 9637-9645.
14. Eilers, J.; van Hest, J.; Meijerink, A.; de Mello Donega, C., Unravelling the Size and Temperature Dependence of Exciton Lifetimes in Colloidal ZnSe Quantum Dots. *J. Phys. Chem. C* **2014,** *118*, 23313-23319.
15. Mourad, D.; Czycholl, G.; Kruse, C.; Klembt, S.; Retzlaff, R.; Hommel, D.; Gartner, M.; Anastasescu, M., Band Gap Bowing of Binary Alloys: Experimental Results Compared to Theoretical Tight-Binding Supercell Calculations for CdxZn1−xSe. *Phys. Rev. B* **2010,** *82*, 165204.
16. Jasieniak, J.; Smith, L.; van Embden, J.; Mulvaney, P.; Califano, M., Re-examination of the Size-Dependent Absorption Properties of CdSe Quantum Dots. *J. Phys. Chem. C* **2009,** *113*, 19468 - 19474.
17. Klimov, V. I.; Mikhailovsky, A. A.; McBranch, D. W.; Leatherdale, C. A.; Bawendi, M. G., Quantization of Multiparticle Auger Rates in Semiconductor Quantum Dots. *Science* **2000,** *287*, 1011-1013.
18. Robel, I.; Gresback, R.; Kortshagen, U.; Schaller, R. D.; Klimov, V. I., Universal Size-Dependent Trend in Auger Recombination in Direct-Gap and Indirect-Gap Semiconductor Nanocrystals. *Phys. Rev. Lett.* **2009,** *102*, 177404-177407.
19. Lin, C.; Gong, K.; Kelley, D. F.; Kelley, A. M., Size-Dependent Exciton-Phonon Coupling in CdSe Nanocrystals Through Resonance Raman Excitation Profile Analysis. *J. Phys. Chem. C* **2015,** *119*, 7491-7498.
20. Lin, C.; Gong, K.; Kelley, D. F.; Kelley, A. M., Electron–Phonon Coupling in CdSe/CdS Core/Shell Quantum Dots. *ACS Nano* **2015,** *9*, 8131-8141.
21. Kelley, A. M.; Dai, Q.; Jiang, Z.-J. B., J. A.; Kelley, D. F., Resonance Raman Spectra of Wurtzite and Zincblende CdSe Nanocrystals. *Chem. Phys.* **2013,** *422*, 272-276.
22. Yu, P. Y.; Cardona, M., *Fundamentals of Semiconductors*. third ed.; Springer: Berlin, 2001.

23. Rogach, A. L.; Kornowski, A.; Gao, M.; Eychmuller, A.; Weller, H., Synthesis and Characterization of a Size Series of Extremely Small Thiol-Stabilized CdSe Nanocrystals. *J. Phys. Chem. B* **1999,** *103*, 3065 - 3069.
24. West, A. R., *Basic Solid State Chemistry*. Wiley Chichester, 1988.
25. Mourad, D.; Czycholl, G., Theory of Band Gap Bowing of Disordered Substitutional II–VI and III–V Semiconductor Alloys. *The European Physical Journal B* **2012,** *85*, 153.
26. Mourad, D.; Czycholl, G., Multiband Tight-Binding Theory of Disordered A x B1- x C Semiconductor Quantum Dots. *The European Physical Journal B* **2010,** *78*, 497-507.
27. Lin, C.; Kelley, D. F.; Rico, M.; Kelley, A. M., The "Surface Optical" Phonon in CdSe Nanocrystals. *ACS Nano* **2014,** *9*, 3928-3938.
28. Bottcher, C. J. F., *Theory of Electric Polarization*. Elsevier: Amsterdam, 1973; Vol. 1.
29. Baker, J. A.; Kelley, D. F.; Kelley, A. M., Resonance Raman and Photoluminescence Excitation Profiles and Excited-State Dynamics in CdSe Nanocrystals. *J. Chem. Phys.* **2013,** *139*, 024702.